

AD-763 757

WAVEGUIDE AND LUMINESCENT PROPERTIES
OF THIN-FILM Pb-SALT INJECTION LASERS

W. H. Weber, et al

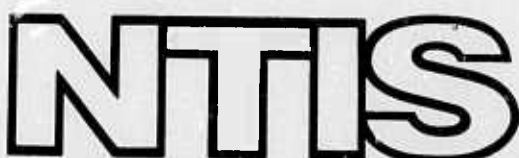
Ford Motor Company

Prepared for:

Naval Research Laboratory
Advanced Research Projects Agency

31 July 1973

DISTRIBUTED BY:



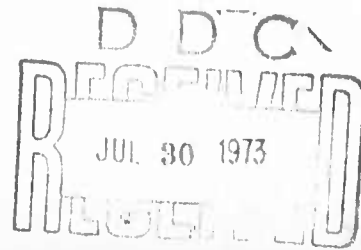
National Technical Information Service
U. S. DEPARTMENT OF COMMERCE
5285 Port Royal Road, Springfield Va. 22151

AD 763752

WAVEGUIDE AND LUMINESCENT PROPERTIES OF
THIN-FILM Pb-SALT INJECTION LASERS

QUARTERLY TECHNICAL REPORT

JULY, 1973



SCIENTIFIC RESEARCH
STAFF

Reproduced by
NATIONAL TECHNICAL
INFORMATION SERVICE
U S Department of Commerce
Springfield VA 22151

PUBLICATION PREPRINT

Prepared for the Naval Research Laboratory under Contract Number
N00014-73-C-0289 - 1 March 1973 to 31 December 1973 ---- \$98,945.

Sponsored by

Advanced Research Projects Agency
ARPA Order No. 2327, Program Code No. 3D10



DISTRIBUTION STATEMENT A
Approved for public release;
Distribution Unlimited

48

WAVEGUIDE AND LUMINESCENT PROPERTIES OF
THIN-FILM Pb-SALT INJECTION LASERS

QUARTERLY TECHNICAL REPORT

JULY, 1973

BY

W. H. Weber*, S. L. McCarthy, M. Mikkor and K. F. Yeung
Ford Motor Company, Scientific Research Staff, Dearborn, Michigan 48121

*Phone: (Area 313) 337-6291

Prepared for the Naval Research Laboratory under Contract Number
N00014-73-C-0289 - 1 March 1973 to 31 December 1973 --- \$98,945.

SPONSORED BY

Advanced Research Projects Agency
ARPA Order no. 2327, Program Code No. 3D10

The views and conclusions contained in this document are those of
the authors and should not be interpreted as necessarily representing
the official policies, either expressed or implied, of the Advanced
Research Projects Agency or the U. S. Government.

Unclassified

Security Classification

DOCUMENT CONTROL DATA - R & D

(Security classification of title, body of abstract and indexing annotation must be entered when the overall report is classified)

1. ORIGINATING ACTIVITY (Corporate author) Scientific Research Staff Ford Motor Company		2a. REPORT SECURITY CLASSIFICATION Unclassified
3. REPORT TITLE Waveguide and Luminescent Properties of Thin-Film Injection Lasers		
4. DESCRIPTIVE NOTES (Type of report and, inclusive dates) First Quarterly Report--1 March 1973 - 30 June 1973		
5. AUTHOR(S) (First name, middle initial, last name) W. H. Weber, S. L. McCarthy, M. Mikkor, K. F. Yeung		
6. REPORT DATE 31 July 1973	7a. TOTAL NO. OF PAGES 44	7b. NO. OF REFS 30
8a. CONTRACT OR GRANT NO. Contract No. N00014-73-C-0289	9a. ORIGINATOR'S REPORT NUMBER(S)	
b. PROJECT NO. ARPA Order No. 2327	9b. OTHER REPORT NO(S) (Any other numbers that may be assigned this report)	
c. Program Code 3D10	d.	
10. DISTRIBUTION STATEMENT Unlimited		
11. SUPPLEMENTARY NOTES Prepared for the Naval Research Laboratory	12. SPONSORING MILITARY ACTIVITY Advanced Research Projects Agency	
13. ABSTRACT <p>We describe the waveguide properties of the asymmetric dielectric slab formed by a very high index film on a low index substrate. The analysis is appropriate for Pb-salt films grown on fluorite structure substrates. The mode reflectivities, surface scattering losses, and gain enhancements for the low order TE and TM modes are considered. The stronger confinement of the TM modes leads to larger gain enhancements and larger scattering losses than for the TE modes of the same order. For the film thicknesses of interest, 2-4 μm, the TE and TM mode reflectivities are comparable.</p> <p>Experimental results are presented for thin-film diode lasers made with Pb Schottky barriers on p-type PbTe (index 6.4) grown epitaxially on BaF₂ substrates (index 1.42). Laser emission at 6.5 μm, both pulsed and cw, is observed at 10-15°K. Well above threshold the spectra generally show two dominant modes spaced by ≈ 1.4 meV. This splitting is explained by a strain induced shift of the energy bands. Using the deformation potentials for PbTe the observed splitting leads to an estimate -2×10^{-4} of the strain component in the [111] direction normal to the film surface. All observed laser lines are TE polarized. An analysis is made of the gain and loss parameters at threshold. The optical gain is estimated from the measured current and quantum efficiency, while the free carrier and reflection losses are calculated from the device parameters. The remaining losses, which we attribute to surface scattering, can then be estimated from the threshold condition. In every case the surface scattering is dominant in establishing the laser threshold, which is consistent with the strong preference shown for TE modes.</p>		

DD FORM 1473 (PAGE 1)
1 NOV 65
S/N 0101-807-6311

IV
Unclassified
Security Classification

A-31408

Unclassified

Security Classification

KEY WORDS	LINK A		LINK B		LINK C	
	ROLE	WT	ROLE	WT	ROLE	WT
Thin-Film Lasers Integrated Optics Optical Waveguides Strain Effects in Epitaxial Films Infrared Diode Lasers						

DD FORM 1 NOV 65 1473 (BACK)
S/N 0101-807-6821

S/N 0101-307-6871

Unclassified
Security Classification

A-31403

SUMMARY

The general goal of this research is to determine the feasibility of an integrated optics technology in the infrared based on IV-VI thin-films grown on fluorite-structure substrates. This materials system has already yielded high-quality photodetectors, lasers, and field-effect transistors. To make useful integrated optical circuits means of waveguiding, coupling, and beam control must also be demonstrated. The eventual goal of the program will be to consider an integrated thin-film heterodyne receiver employing grating couplers and an injection laser as a local oscillator. The primary emphasis during the initial phase of this research has been the development of a theoretical understanding of waveguiding in a very high index film on a low index substrate and the application of this theory to thin-film injection lasers. This work will form the basis for subsequent analyses of other waveguide structures or integrated optics devices in these materials. Calculations have been done for a PbTe film, index 6.4, on a BaF₂ substrate, index 1.42. The mode reflectivities at the termination of the guide, the surface scattering losses due to surface imperfections, and the gain (or loss) enhancement associated with intrinsic amplification (or attenuation) in the film are considered for the low order TE and TM modes. The two types of modes have comparable reflectivities for film thicknesses of interest, 2-4 μm . The gain enhancement is substantially higher for the TM modes owing to their stronger optical confinement. The surface scattering loss for the TM modes is also higher than for TE modes of the same order. The magnitude of the surface loss, however, depends on an unknown surface roughness parameter σ , the variance of the surface height.

An analysis is made of the gain and loss parameters at threshold for PbTe lasers made with Pb Schottky barriers on p-type films. The optical gain is estimated from the measured current and quantum efficiency, while the free carrier and reflection losses are calculated from the device parameters. The analysis suggests that the surface scattering loss is dominant in establishing the laser threshold. Consistent with this suggestion is the observation that the laser modes are always TE polarized. A crude theory of surface scattering losses leads to an upper limit on σ of .03-.06 μm .

The laser emission spectra generally show two dominant modes spaced by about 1.4 meV. This splitting is several times larger than the Fabry-Perot mode spacing, and we have attributed it to a strain-induced shift of the energy band. The strain in the PbTe film arises because its thermal expansion coefficient is slightly different from that of the BaF_2 substrate. Using a deformation potential calculation leads to an estimate -2×10^{-4} for the strain component in the [111] direction normal to the film surface.

Post-growth fabrication procedures for the thin-film PbTe lasers are described. These include annealing the films for a few days at 350°C in a Te atmosphere and defining the laser cavity with a photoresist etching technique before depositing the usual metallic contacts.

I. INTRODUCTION

Laser action in the Pb-salts was first observed in 1964 by J. F. Butler et al.,¹ who reported diode lasers in PbTe. Subsequently, laser diodes have been made in PbSe² and PbS³ as well as in most of the pseudo-binary alloys such as $Pb_{1-x}Sn_xTe$ and $Pb_{1-x}Sn_xSe$.⁴ These lasers have been made from bulk crystalline samples grown by vapor transport or Bridgman techniques, and a review of this work is given in a recent paper by Harman.⁵ The bulk devices consist of a rectangular crystal with cleaved (100) end faces forming a Fabry-Perot cavity. Due to the weak confinement of the laser beam in the direction normal to the junction plane (typically 40-50 μm at liquid He temperatures), these devices approximate a volume laser with nearly plane wave propagation assumed between the end reflectors. Previous analyses of the gain and loss characteristics of these lasers have generally used the volume laser approximation.⁵⁻⁷

Recent studies of the epitaxial growth of IV-VI compounds on fluorite structure substrates have shown that films of excellent crystalline quality can be achieved.⁸ These films have yielded high quality infrared detectors⁹ and field-effect transistors as well as lasers.¹⁰ The primary purpose of this paper is to discuss the light emission and laser characteristics of the thin-film lasers. Since typical film thicknesses are several microns, i.e., on the order of the emission wavelength, the waveguiding properties of the films must be considered in determining the mode preferences and threshold conditions for the lasers. The increased electrical and optical confinement afforded by the thin films

enhances the optical gain significantly over that obtained in bulk devices.

At the same time, however, the cavity losses are increased by the introduction of surface scattering.

In Section II we present an analysis of the properties of the asymmetric dielectric waveguide formed by a high index semiconductor film on a low index substrate. Surface scattering losses, reflection losses, and gain enhancement for the low order TE and TM modes are considered. Calculations are presented for PbTe films, index 6.4, on BaF_2 substrates, index 1.42, but the results should apply to other systems with comparably large index differences. The stronger optical confinement associated with the TM modes can lead to reflectivities and gain enhancements larger than those for the corresponding TE modes. On the other hand the TE modes always show lower surface scattering losses than TM modes of the same order. To treat these surface losses we will use the simple theory of Tien based on the Rayleigh criterion.¹¹⁻¹² This theory involves a single unknown parameter σ , the variance of the surface height, which we assume to be the same for both surfaces. For the mode reflectivity calculations we will use an extension of the method employed by Reinhart et al. to treat a similar problem in double heterostructure lasers.¹³ For thick films we find results very similar to theirs, with the TE modes showing higher reflectivities than the TM modes. For thinner films, however, there is no clear preference.

We present the experimental results in Section III. These include a brief description of the sample preparation, an analysis of the spontaneous emission spectrum at 77°K, and measurements of the spectra

and polarization of the laser emission at liquid He temperatures. An important step in the sample preparation, which was not used in previous devices,¹⁰ is the use of a photoresist etching technique to define the ends of the optical cavity. This produces much better edges than those obtainable on the as-grown films using close-spaced evaporation masks. Minority carrier injection is achieved with Pb Schottky barriers on p-type PbTe films. The spontaneous emission spectrum is fit quite well with the band-to-band recombination model assuming vertical transitions. Under high-current conditions at liquid He temperatures, some devices show two distinct laser emission lines with a separation much larger than the cavity mode spacing. This splitting is explained in terms of a strain induced shift of the energy bands. Using a deformation potential calculation leads to the estimate -2×10^{-4} for the strain component normal to the film surface.

In the last Section we give an analysis of the gain and loss parameters at the lasing threshold. The optical gain at threshold is estimated from the diode current using the band-to-band recombination model. The free carrier absorption is calculated from the measured material parameters, and the reflection losses are determined from the results of Section II. Using these results the surface scattering loss can be estimated, assuming there are no other loss mechanisms. This analysis gives an upper limit for c in the range .03-.06 μm . In all cases the estimated gain at threshold is much greater than the sum of the free carrier and reflection losses. This indicates that the additional losses, which we attribute to surface scattering, are dominant in determining the laser threshold.

II. WAVEGUIDE PROPERTIES

A. Description of the Modes

Since the general formalism for treating the waveguide modes of the asymmetric dielectric slab is well known,^{11,14} we will omit derivations and give only those results essential for defining the notation and understanding the subsequent discussion. For the 2-dimensional geometry shown in Fig. 1 the guided modes follow from the solutions of the homogeneous Maxwell equations which vanish at $z = \pm \infty$. The solutions separate into transverse electric (TE) and transverse magnetic (TM) modes. The appropriate equation for the TE modes is

$$\left(\frac{d^2}{dz^2} + n_i^2 \frac{\omega^2}{c^2} \right) E_y = \beta^2 E_y , \quad (1)$$

where β is the propagation constant in the x direction, n_i is the refractive index of the i^{th} medium, E_y is the electric field strength (which has only a y component), ω is the angular frequency, and c is the velocity of light. In our problem, with the refractive index stepwise constant in all directions, H_y for TM modes also satisfies Eq. (1).

The solutions result from matching the boundary conditions at the dielectric interfaces and solving the resulting eigenvalue equation. Following Tien,¹¹ the transverse field components for TE and TM modes can be written in the form:

$$A e^{i(\beta x - \omega t)} \begin{cases} \cos(k_2 z_{12}) e^{-k_1(z-z_{12})} & z > z_{12} , \\ \cos(k_2 z) & z_{12} > z > -z_{23} , \\ \cos(k_2 z_{23}) e^{k_3(z+z_{23})} & -z_{23} > z , \end{cases} \quad (2)$$

where z_{12} and $-z_{23}$ are the values of z at the upper and lower surfaces,

respectively; $k_{1,3} = (\beta^2 - n_{1,3}^2 k^2)^{\frac{1}{2}}$; $k_2 = (n_2^2 k^2 - \beta^2)^{\frac{1}{2}}$; and we have introduced the free space wave vector $k = \omega/c = 2\pi/\lambda$. The allowed values of the propagation constant β are determined from the equation

$$z_{12} + z_{23} = d , \quad (3)$$

where d is the film thickness. For the TE modes z_{12} and z_{23} are given by

$$\begin{aligned} k_2 z_{12} &= \arctan(k_1/k_2) , \\ k_2 z_{23} &= \arctan(k_3/k_2) + m\pi , \end{aligned} \quad (4)$$

while for the TM modes we have

$$\begin{aligned} k_2 z_{12} &= \arctan(n_2^2 k_1/n_1^2 k_2) , \\ k_2 z_{23} &= \arctan(n_2^2 k_3/n_3^2 k_2) + m\pi , \end{aligned} \quad (5)$$

where $m = 0, 1, 2, \dots$, is the mode index. The roots of Eq. (3) are generally found by numerical techniques. Note that defining the fields by expression (2) requires the position $z = 0$ be different for each mode.

We show in Fig. 2 plots of the propagation constant β as a function of the guide thickness d for the first three TE and TM modes. The frequency used in these calculations corresponds to a free space wavelength of $6.5 \mu\text{m}$. Also shown as dashed curves are plots of the equation

$$d = \frac{(m+1)\pi}{(n_2^2 k^2 - \beta^2)^{\frac{1}{2}}} , \quad (6)$$

which would describe the solutions for a waveguide with perfectly conducting walls, i.e., no penetration of the fields into the surrounding media. The purpose of these plots is to indicate that for most values of β the TM modes are very closely fit by Eq. (6) and are, thus, much more strongly confined than the TE modes. This feature leads to important differences in the mode reflectivity and gain enhancement as we will demonstrate in the remainder of this section.

B. Mode Reflectivity

To determine the exact reflectivity of a waveguide mode requires the solution of a difficult boundary value problem, and no attempt at such a solution will be given here. Instead, we will use a physical optics argument to obtain an estimate of the reflectivity. This method is the same as one used previously to estimate the mode reflectivities in double-heterostructure lasers.¹³ Our results will differ from that work in two respects: We will use the exact mode profiles in the calculations, rather than a Hermite-Gaussian approximation; and we will introduce a truncated Fourier transform to take into account the evanescent tails of the modes extending into the surrounding media.

We assume the semiconductor film is terminated with a surface in the z-y plane. The incident field illuminating the guide end is written as a Fourier decomposition $S(k_z)$ in the z direction of the transverse field component. For a TE mode we define $S(k_z)$ by

$$S(k_z) = \int_{-\infty}^{\infty} E_y(z) e^{-ik_z z} dz . \quad (7)$$

Each Fourier component corresponds to a plane or evanescent wave incident on the film-air boundary at the guide end. The evanescent tails on $E_y(z)$, however, will not "see" the end of the guide as effectively as the rest of the mode. To take this effect into account, we introduce a truncated transform:

$$S_t(k_z) = \int_{-z_2}^{z_1} E_y(z) e^{-ik_z z} dz . \quad (8)$$

We can now find the reflected fields by multiplying each of these components by the appropriate Fresnel coefficient $F(k_z)$. This method assigns zero reflectivity to the evanescent tails and will probably underestimate the total reflected wave. We expect it to be a very good approximation for large d , and for small d it is a physically reasonable way of treating the mode reflectivities near cutoff. Finally, the amplitude reflectivity r is given by projecting out the original mode from the reflected waves:

$$r = \int_{-\infty}^{\infty} S^*(k_z) F(k_z) S_t(k_z) dk_z / \int_{-\infty}^{\infty} S^*(k_z) S_t(k_z) dk_z . \quad (9)$$

The Fresnel coefficient for TE modes is given by

$$F_{TE}(k_z) = (\mu_2 - \mu_1) / (\mu_2 + \mu_1) , \quad (10)$$

where $\mu_i = (n_i^2 k^2 - k_z^2)^{1/2}$. For the TM modes we replace $E_y(z)$ by $H_y(z)$ and use the Fresnel coefficient F_{TM} :

$$F_{TM}(k_z) = (n_1^2 \mu_2 - n_2^2 \mu_1) / (n_1^2 \mu_2 + n_2^2 \mu_1) . \quad (11)$$

In Fig. 3 we show computer results for the mode reflectivities of the first two TE and TM modes, calculated using Eqs. (7) - (11). The integrals in Eqs. (7) and (8) can be evaluated explicitly, but the one in Eq. (9) must be done numerically.

For thick films the simple formulas in Ref. 13 give roughly the same results, e.g., the reflectivity values of the zero order modes at $d = 6 \mu\text{m}$ are within 10% of those in Fig. 3. However, for the data we will be presenting typical values are $d = 2-4 \mu\text{m}$, and for this range of thicknesses the results from the two models are very different.

It is also of interest to consider the reflectivity of a guide with a nonrectangular end. Films grown by evaporation through a mask will tend to have a tapered edge due to the finite source size and the separation between substrate and mask. We assume this fuzzy edge can be approximated by a plane surface whose normal is in the x-z plane making a small angle ν with the x axis. It is then a simple matter to modify Eq. (9) for this model. The resulting reflectivity as a function of ν is shown in Fig. 4 for the zero order modes of a $4 \mu\text{m}$ film. For thinner films the reflectivity falls off less rapidly and for thicker films more rapidly than shown in the figure. We have found that an edge defined by an evaporation mask will tend to have a tapered region at least one micron wide, and it is clear from Fig. 4 that such an edge will introduce severe reflection losses. To get around this problem we have been using an etching technique to define the laser edges.

C. Surface Scattering Losses

We will treat the surface scattering losses using the simple theory based on the Rayleigh criterion for reflection losses from slightly rough surfaces.^{11,16} Although this theory is fairly crude in that it ignores the mode properties of the guide, it is based on sound physical arguments

and is easy to apply. In addition, it is the only theory that has been successfully applied to experiments on losses in an optical waveguide.¹²

To calculate the loss we first decompose the transverse field component inside the guide into two plane waves:

$$A e^{i(\beta x - \omega t)} \cos(k_2 z) = \frac{A}{2} \{ e^{i(\beta x + k_2 z - \omega t)} + e^{i(\beta x - k_2 z - \omega t)} \}$$

The power in each plane wave is reduced after a single reflection by the factor $\exp\{-(4\pi n_2 \sigma \cos \theta_2 / \lambda)^2\}$, where σ is the variance of the surface height, assumed to be the same for both surfaces, $\theta_2 = \arctan(\beta/k_2)$ is the angle of incidence measured from the normal, and λ is the free space wavelength. Using this method one can show that the power attenuation coefficient α_s for both TE and TM modes can be written in the form:

$$\alpha_s = \left(\frac{4\pi n_2 \sigma}{\lambda} \right)^2 \frac{\cos^3 \theta_2}{\sin^2 \theta_2} \frac{1}{d_{\text{eff}}} , \quad (12)$$

where d_{eff} is given by

$$d_{\text{eff, TE}} = d + k_1^{-1} + k_3^{-1} , \quad (13)$$

$$d_{\text{eff, TM}} = d + \frac{n_1^2 n_2^2}{k_1} \frac{k_1^2 + k_2^2}{n_1^4 k_2^2 + n_2^4 k_1^2} + \frac{n_2^2 n_3^2}{k_3} \frac{k_2^2 + k_3^2}{n_3^4 k_2^2 + n_2^4 k_3^2}$$

The quantity d_{eff} describes the effective spatial extent of a mode in the z direction. The expressions (13) are derived by considering the power flow. For a mode far away from cutoff d_{eff} will nearly equal d . As a mode approaches cutoff, however, d_{eff} rapidly diverges.

We show in Fig. 5 the surface scattering loss coefficients as a function of film thickness calculated from Eqs. (12) and (13). Ignoring the sharp drops in the losses at cutoff, the TE_0 mode shows the lowest loss for all d values of interest.

D. Gain Enhancement

Optical gain in a semiconductor is obtained by population inversion induced through minority carrier injection. This population inversion contributes a small negative imaginary component $\delta\epsilon$ to the dielectric constant. The gain coefficient for plane waves α_p resulting from $\delta\epsilon$ is given by

$$\alpha_p = \frac{k}{n_2} \delta\epsilon . \quad (14)$$

In a waveguide the gain coefficient for a mode will differ from the plane wave result for two reasons: 1. The guided mode can be viewed as taking a zig-zag path down the film. This will increase the effective path length and, thus, will increase the gain coefficient. 2. The guided mode has evanescent tails extending into the surrounding passive media. This mode leakage effect will tend to decrease the gain.

To calculate the gain coefficient we observe that Eq. (1) is identical in form to the one-dimensional Schroedinger equation for a particle in a square well.¹⁷ This means we can use first order perturbation theory to calculate the change in the eigenvalue β^2 caused by a small change in the index. The result for TE modes is

$$\delta(\beta^2) = \int_{-\infty}^{\infty} |E_y|^2 \delta\epsilon(w^2/c^2) dz / \int_{-\infty}^{\infty} |E_y|^2 dz . \quad (15)$$

Since the minority carrier diffusion length is typically an order of magnitude larger than the film thickness, we can assume that $\delta\epsilon$ is uniform across the guide. With this simplification we can write the gain enhancement factor G , defined to be the gain coefficient for the mode α divided by that for a plane wave, in the following form:

$$G = \frac{\alpha}{\alpha_p} = \frac{n_2 k}{\beta} \frac{\int_{-z_2}^{z_1} |E_y|^2 dz}{\int_{-\infty}^{\infty} |E_y|^2 dz} . \quad (16)$$

The same formula applies for TM modes when $E_y(z)$ is replaced with $H_y(z)$.

The first factor in Eq. (16) is always greater than unity, while the second is always less than unity.

Evaluating the integrals in Eq. (16) leads to the following expressions for G

$$G_{TE} = \frac{n_2 k}{\beta} \frac{d + \frac{k_1}{k_1^2 + k_2^2} + \frac{k_3}{k_3^2 + k_2^2}}{d_{eff, TE}} , \quad (17)$$

$$G_{TM} = \frac{n_2 k}{\beta} \frac{d + \frac{n_2^2 n_1^2 k_1}{n_2^4 k_1^2 + n_1^4 k_2^2} + \frac{n_2^2 n_3^2 k_3}{n_2^4 k_3^2 + n_3^4 k_2^2}}{d_{eff, TM}} .$$

These expressions are plotted in Fig. 6 for the first two modes. Note that the TM modes show substantially more gain enhancement than the TE modes. This results from the stronger optical confinement associated with the TM modes.

III. EXPERIMENTAL

A. Sample Preparation

PbTe films are grown epitaxially on cleaved (111) BaF₂ substrates. The details of this growth technique and the characterization of the films have been described previously.⁸ Hall effect measurements are used to determine the carrier concentrations and mobilities. The as-grown films are p-type with $p = 6 \times 10^{16} - 4 \times 10^{17} \text{ cm}^{-3}$. Typical mobilities at 10°K are $2-5 \times 10^4 \text{ cm}^2/\text{V-sec}$, and typical film thicknesses are 2-4 μm .

Since it is not possible to produce cleaved end faces on the thin-films, as is normally done with bulk devices, we have developed a photoresist etching technique to produce Fabry-Perot cavities with nearly square ends. The laser cavity is formed by first depositing a dumbbell shaped mask on the PbTe film with Shipley AZ-111 photoresist. The exposed PbTe is etched away with an HBr:Br, 10:1, solution in an equal volume of water. The photoresist is then removed, and a $\sim 4000\text{\AA}$ Pt film is sputtered onto the ends of the dumbbell forming the ohmic contacts. Finally, $\sim 2000\text{\AA}$ Pb strips 150-400 μm wide are evaporated across the PbTe forming the Schottky barriers. The Pb is evaporated at an angle of 45° with respect to the film normal. This procedure serves two purposes: It gives a better electrical connection across the sharp edge of the film on one side, and it leaves the other side bare permitting the light to exit. A schematic drawing of a completed sample is shown in Fig. 7.

The samples are mounted with a thermal conducting epoxy on copper plates connected directly to the cold finger of a liquid helium dewar. The plates are positioned with the dumbbell vertical and the light emitted

within a cone of half-angle 17° centered roughly 20° from the plane of the substrate is collected and focused onto the entrance slit of a grating spectrometer. This sample orientation provides maximum light collection efficiency. The light at the exit slit is focused onto a Ge:Au liquid N₂-cooled conductor. For pulsed operation the current pulses are 2 μ sec long at a repetition rate of a few kHz and boxcar integration is used. For cw operation the light at the entrance slit is mechanically chopped at 350 Hz and synchronous detection is used.

The importance of using an etching technique to define the laser end reflectors is demonstrated in Fig. 8. Here we show scanning electron microscope photographs of the cross sections of two laser ends--one prepared as described above, the other defined by a close-spaced evaporation mask. The guide end for the etched sample is normal to the substrate to within the accuracy that we can measure it. For the other sample, however, the guide end deviates from normal by an angle $\nu \approx .5$ rad, which would lead to a power reflectivity for a zero order mode several orders of magnitude below that for an ideal end reflector.

Normally a Schottky barrier diode is a majority carrier device leading to the recombination of majority carriers at the metal surface with little or no light emission. A Pb film on p-type PbTe, however, produces an n-type inversion layer which can lead to electron injection. Nill et al. have shown that under high forward bias this structure is apparently as efficient at injecting minority carriers as a normal p-n junction.^{18,19} This result is consistent with our estimates of the internal quantum efficiency η for spontaneous emission at low temperature.¹⁰ We find in our devices a value for η of about one percent, while the best bulk p-n junctions yield values in the range 1-5%.

B. Spontaneous Emission at 77°K

Previous measurements of both photoluminescence²⁰ and electroluminescence¹⁰ in PbTe indicate that the emission arises from direct band-band recombination with k -conservation, i.e., only near-vertical transitions are allowed. The primary evidence for this interpretation from our data is the observation of a highly asymmetric lineshape with a sharp cutoff at the bandgap on the low energy side of the peak and a long tail on the high energy side. The impurity banding, non- k -conservation model of Lasher and Stern²¹ has been used to interpret emission from PbSe.²² However, this model predicts a more symmetric lineshape with a substantial tail extending to energies less than the bandgap, which does not give a good fit to our data. We will, thus, restrict our discussion to the k -conservation model. For PbTe this model yields the following expression for the total spontaneous emission rate as a function of the energy E :^{21,23}

$$r_{sp}(E) = A(E-E_G)^{\frac{1}{2}} f_c(\frac{1}{2}E-\frac{1}{2}E_G+E_c) \{1-f_v(\frac{1}{2}E_G-\frac{1}{2}E+E_v)\} , \quad (18)$$

where

$$A = \frac{4n_2 e^2 E G m_d^{\frac{1}{2}} (m_d + m_o)}{m_o^5 \hbar c^5 \pi^2} ;$$

$m_d = .052 m_o$ is the density of states effective mass,²⁴ which is taken to be the same for both bands;²² E_c and E_v are the conduction and valence band edges, respectively; $E_G = E_c - E_v$ is the bandgap; m_o is the free electron mass; f_c and f_v are the Fermi occupation probabilities for electrons in the conduction and valence bands, respectively:

$$f_c(E) = \frac{1}{1 + \exp\{(E - \mu_c)/kT\}} , \quad f_v(E) = \frac{1}{1 + \exp\{(E - \mu_v)/kT\}} ; \quad (19)$$

and μ_c , μ_v are the respective quasi-Fermi levels of the conduction and valence band. The dimensions of $r_{sp}(E)$ are $eV^{-1}cm^{-3}sec^{-1}$.

The experimentally observed spectrum $I(E)$ will be modified by re-absorption. The emission from each increment of volume a distance x from the exit face is attenuated by the factor $\exp(-\alpha x)$, where α is the attenuation coefficient. Integrating over x leads to a lineshape $r_{sp}(E)/\alpha(E)$. However, $r_{sp}(E)$ and $\alpha(E)$ are related by²¹

$$\alpha(E) = \frac{\pi^2 c^2 \hbar^3}{n_2^2 E^2} (e^{(E - \mu_c + \mu_v)/kT} - 1) r_{sp}(E). \quad (20)$$

At 77°K for the range of carrier concentrations and injection levels we are considering, we find that the 1 in Eq. (20) can be neglected compared with the exponential. Thus, for our experimental conditions, the lineshape is dominated by a simple Boltzmann factor:

$$I(E) \propto e^{-E/kT}. \quad (21)$$

Eqs. (18) and (20) predict a vertical drop in the intensity from its maximum at the band edge. Actually, this corner will be slightly rounded due to the residual attenuation such as free carrier absorption which does not vanish at this energy.

We show in Fig. 9 an emission spectrum at 77°K along with the predicted curve. A better way of presenting the data is shown in Fig. 10 for a different sample where we plot $\ln(I/I_{peak})$ vs E above the peak. In both cases, the agreement with Eq. (21) is good. Although the samples used

for these data have carrier concentrations differing by a factor of three, the emission lineshapes are essentially the same. In order to observe a change in the linewidth with carrier concentration as was done in the photoluminescence experiments,¹⁹ it is necessary to use higher carrier concentrations and higher injection levels.

It is important to note that the lineshape predicted by Eq. (21) in no way depends on the band parameters or carrier concentrations. In fact it does not distinguish electron from hole recombination. In a previous paper, however, we presented data with the light collected through the BaF₂ substrate normal to the film.¹⁰ For that case the reabsorption correction is very small since the light has on the average a very short path length through the film. The emission spectrum is broader than it is here, and Eq. (18) with the appropriate effective mass and carrier concentration must be used to fit the data.

Polarization measurements of the spontaneous emission indicate that both polarizations have identical lineshapes with the TE intensity (E in the plane of the substrate) being about a factor of two larger than the TM intensity. We have not been able to obtain good spontaneous emission spectra at liquid He temperatures. Generally the spectra begin to show stimulated line narrowing at about the same current levels that produce measurable signals through the spectrometer with sufficient resolution.

C. Laser Emission at 10-15°K

Lasing was first observed in these films under pulsed conditions at 12°K with a threshold current of several hundred milliamperes for a typical device -- a typical device being 400 μm wide and 4 μm thick with $p \approx 10^{17} \text{ cm}^{-3}$. Our best diodes now lase with a threshold current of a few tens of milliamperes. The primary improvement we have made is the use of the photoresist etching technique to define the laser cavity. We have also done some preliminary studies which indicate that the laser performance can be improved by post-growth annealing at $\sim 350^\circ\text{C}$ in a Te atmosphere which increases the carrier concentration to the high 10^{17} or low 10^{18} range. Besides increasing the carrier concentration and mobility, the annealing apparently improves the quantum efficiency.

An example of the cw laser emission from one of our annealed samples is shown in Fig. 11. This device is 2.4 μm thick with a cavity length $L = 400 \mu\text{m}$. The laser threshold is about 30 mA, corresponding to the upper trace in Fig. 11. The widths of all the lines in the figure are spectrometer resolution limited. The 100 mA trace shows a complicated mode spectrum with seven discernible modes. The four at longer wavelengths show a common mode spacing of $\sim 80\text{\AA}$. The three remaining modes do not appear to show a common spacing. However, if we insert the 30 mA peak position into the mode pattern at 100 mA, then we again have a set of four modes with an 80\AA spacing as indicated by the arrows in Fig. 11.

Using the mode spacing formula for a plane-wave Fabry-Perot cavity, the effective refractive index $n_{\text{eff}} = n - \lambda(dn/d\lambda)$ corresponding to the data in Fig. 11 would be 6.3. Actually, the different waveguide modes will have different effective indices, and we should take this into

account. The mode effective indices will always be less than the film effective index. Thus, the use of the plane-wave Fabry-Perot formula will underestimate n_{eff} for the film. For example, if we assume a TE_0 mode for the data in Fig. 11, then n_{eff} would be 6.4 instead of 6.3. We have observed effective indices in some films as large as 8. Such a wide spread in this quantity is not surprising, however, considering the large dispersion in $n_2(\lambda)$ near the band edge in PbTe reported by Zemel *et al.*²⁵ at low temperatures.

The observation of two or three separate sets of Fabry-Perot spaced modes occurs in most devices at currents well above threshold. The reason for this is not clear. It could be due to inhomogeneities in the film or on the surface which produce laser filaments in the transverse direction.

All of the laser lines shown in Fig. 11 are polarized $\approx 100\% (\pm 5\%)$ with the electric vector in the plane of the substrate, indicating pure TE modes. In fact, we have measured the polarization of 30-40 modes in several different diodes and have invariably found them to be TE polarized, although occasionally the polarization is only 60-80% TE. The observation of modes which are only partially polarized may be another indication of filamentation, since any strong confinement in the direction along the film will lead to modes with mixed TEM polarization. The only cavity property that strongly favors TE modes is the surface scattering loss, thus our results would suggest that this loss mechanism is the dominant one in establishing the laser threshold.

In most samples we observe two prominent laser lines with a separation large compared with the cavity mode spacing. This feature usually occurs well above threshold and often only under pulsed conditions. One example is shown by the separation between the two dominant modes in the lower trace in Fig. 11. Another example is shown in Fig. 12

for a different sample. The small splitting of the longer wavelength modes in this figure is the cavity mode spacing. We have interpreted the large splitting as arising from a strain-induced shift of the energy bands.

The thermal expansion coefficient of the substrate is less than that of the film. This means that at low temperatures the film will appear stretched in the plane of the substrate, the (111) plane, and compressed in the direction normal to it. This deformation will partially remove the degeneracy of the various conduction and valence bands. Since the band gap in the Pb-salts is at the zone boundary in the [111] direction, the bands which are oriented along [111] will shift differently from those along [111], [111], and [111], which remain degenerate.

To estimate the difference between the bandgap at (111) and that at the other three points, we will assume the deformation of the crystal is equivalent to that produced by a stress S applied uniformly in the directions parallel to the (111) plane. For this stress configuration the strain tensor ϵ'_{ij} in the coordinate system with the z' axis in the [111] direction will be diagonal with nonzero components: $\epsilon'_{11} = \epsilon'_{22} = (s'_{11} + s'_{12}) S$ and $\epsilon'_{33} = 2s'_{31} S$, where s'_{ij} are the elastic compliance constants in the primed coordinate system. This description is, of course, not exact, since the actual strain will vary over the thickness of the film. In a thin film, however, we can consider the strain values to be averaged over the thickness. Once the strain tensor is known, the shift of any band edge can be determined by $\Delta E = D_{ij} \epsilon_{ij}$, where the D_{ij} are the appropriate components of the deformation potential tensor.²⁶ After transforming ϵ'_{ij} into the coordinate system with the cubic crystal axes and using the expressions for D_{ij} given by McMullin,²⁷ we find

that the difference between the two bandgaps in PbTe can be written in the form:

$$\Delta E_G = \frac{8\epsilon'_{33}(\beta_c - \beta_v)}{1 - 2c_{44}/(c_{11} + 2c_{12})} \approx 6.4 \epsilon'_{33} (\text{eV}), \quad (22)$$

where ϵ'_{33} is the strain in the [111] direction; β_c and β_v are the off-diagonal elements of the deformation potential tensor for the conduction and valence bands, respectively; and the c_{ij} are the standard elastic stiffness constants. We have used the numerical values for these constants summarized in Ref. 27. Our experimental value of the energy gap difference is $\Delta E_G = 1.4 \text{ meV} \pm 30\%$, corresponding to a strain $\epsilon'_{33} \approx -2.2 \times 10^{-4}$.

Recently Hohnke has measured the temperature dependence of the strain component ϵ'_{33} for similarly grown PbSe films on BaF₂ substrates.²⁸ He finds that at 77°K $\epsilon'_{33} \approx -3.3 \times 10^{-4} \pm 10\%$, which is fairly close to the value we would predict from the emission spectra for PbTe. This result is not surprising, however. Since the thermal expansion coefficients for PbTe and PbSe are nearly equal, we would expect the low temperature strains in the two materials to be similar.

IV. THRESHOLD ANALYSIS AND DISCUSSION

In this section, we present an analysis of the gain and loss parameters which characterize the laser threshold. The analysis will necessarily be very crude since we have no way of independently measuring the various contributions separately. The threshold condition we can write in the form

$$-G\alpha(E_m) = G \alpha_{fc} + \alpha_s + L^{-1} \ln R^{-1}, \quad (23)$$

where α_{fc} is the free carrier absorption, α_s is the surface scattering loss, G is the gain enhancement factor, L is the cavity length, R is the power reflectivity, and $\alpha(E_m)$ is the maximum plane-wave gain coefficient given by Eqs. (18) and (20). Under lasing conditions $\alpha(E_m)$ will, of course, be negative. The free carrier and reflection losses can be estimated reasonably well, but the surface scattering loss α_s involves an unknown scaling parameter, the variance of the surface height. On the other hand, the maximum gain coefficient $\alpha(E_m)$ can be related to the threshold current in the diode by

$$I_t = (eV/\eta) \int r_{sp}(E) dE, \quad (24)$$

where I_t is the threshold current, V is the recombination volume, and η the internal quantum efficiency. Thus the least known parameter in Eq. (23) is the surface scattering loss, and our aim will be to use estimates of the other quantities to determine it.

Normally Eq. (24) is written with the current density j on the left and the minority carrier diffusion length on the right. That way of expressing the j vs $\alpha(E_m)$ relation is appropriate for a bulk p-n junction with the current flow uniform and normal to the junction plane. In our diodes the current flow is non-uniform with components both normal and transverse to the junction plane. To make the problem tractable we will make two simplifying assumptions: First, we assume that electron injection occurs predominantly at the edge of the Pb film. This should be a good approximation at high injection when the junction voltage is large compared with kT/e , since the voltage drop along the film will substantially reduce the injection away from the Pb edge nearest the Pt contact. Second, we assume that the electron distribution is uniform in the z and x directions and spread out by the diffusion length in the y direction. This should be a good approximation at low temperatures where the minority carrier diffusion length L_n is roughly an order of magnitude greater than the film thickness. Our entire analysis of the waveguiding properties implicitly assumes that lasing begins not in the region covered by the Pb film, but in the region adjacent to it. This will certainly be the case near threshold where the additional losses of the metal film would preclude lasing in that region. Thus the recombination volume V is a rectangular region with thickness d , width L_n , and length L . The accepted value for the minority carrier diffusion length in Pb-salt lasers is roughly $20 \mu\text{m}$,^{5,6} but we will take $L_n = 40 \mu\text{m}$ since the carriers can diffuse in both the plus and minus y directions.

In the spirit of our approximate treatment we will use a simplified expression for estimating the optical gain at threshold rather than the integral relation (24). This simple expression can be written in the form²³

$$-\alpha(E_m) = \frac{I_t \eta \pi^2 c^2 n^3}{e V n_2^2 \gamma E_m^2 \Delta E} , \quad (25)$$

where γ is the "demcrit" factor and ΔE is a measure of the spontaneous linewidth. We have found that using $\gamma \Delta E = 4.3$ meV in Eq. (25) leads to a value which is always within about 20% of the value calculated from Eq. (24) for a particular threshold condition. The quantum efficiency was measured previously to be about one per cent for unannealed samples.¹⁰

In Table 1 we show typical threshold data for four PbTe lasers. The threshold current is determined by examining both the emission spectrum and the variation of the light intensity with current. The uncertainty in this determination is about 10%. The optical gain is calculated from Eq. (25) with $\eta = 1\%$ and $\gamma \Delta E = 4.3$ meV. The free carrier absorption coefficient is calculated from²⁹

$$\alpha_{fc} = \frac{p c^3 \lambda^2}{4 \pi^2 n_2^2 c^3 \epsilon_0 \mu_p m_c^2} , \quad (26)$$

where $m_c = 0.032 m_o$ is the conductivity effective mass²⁰; p and μ_p are the hole carrier concentration and mobility, which are measured for each device; and ϵ_0 is the free space dielectric constant. The reflection loss is determined from Fig. 3 assuming a TE_0 mode. The surface scattering loss is determined from the threshold condition (23) using a gain enhancement factor of unity. The value of σ is calculated from Fig. 5, again assuming a TE_0 mode. In every case α_s is the dominant loss contribution. This is

consistent with the observed strong preference for TE modes. The values for σ given in the table should be considered as upper limits since we have probably overestimated the carrier confinement by the assumption of a line source of injection and there may indeed be other losses which we have overlooked. In the absence of an experimental verification of the surface loss theory and its applicability to our films, it is more appropriate to view σ as a phenomenological parameter characterizing the surface loss, rather than a true measure of the variance of the surface height.

Annealed samples show a factor of 3-5 lower threshold currents than unannealed ones. Presumably this results from an increase in η , in which case the predicted values of σ for those samples would again be the same magnitude as those shown in Table 1. Annealing also produces a shift of about 2% of the laser emission to higher energies. An example of this shift can be seen by comparing Figs. 11 and 12. The shift arises from the increase in carrier concentration. With higher hole concentrations higher energy transitions are allowed. These transitions involve a larger density of states than those closer to the band edges and, thus, will tend to be favored for lasing.

The primary conclusion we can draw from this threshold analysis is that there are large losses in addition to free carrier and reflection losses which are important in determining the laser threshold. Significant improvements in the laser performance can be expected if these losses are reduced. Coupled with the increased quantum efficiency from annealing, laser thresholds as low as 1 mA should be attainable in our devices. In addition a high-gain, single-pass optical amplifier could be made by eliminating the end reflectors and adding input and output grating couplers at the ends of the active region.

ACKNOWLEDGMENTS

We are indebted to H. Holloway, E. M. Logothetis, and A. J. Varga for participating in the development of the device fabrication techniques which made this research possible. We would also like to thank D. K. Hohnke, P. V. S. Rao, and S. W. Kaiser for providing us with samples and with expert technical advice regarding the annealing, etching, and other device preparation procedures and Professor G. W. Ford for several discussions regarding the mode reflectivity calculations.

REFERENCES

1. J. F. Butler, A. R. Calawa, R. J. Phelan, Jr., T. C. Harman, A. J. Strauss, and R. H. Rediker, *Appl. Phys. Letters* 5, 75 (1964).
2. J. F. Butler, A. R. Calawa, R. J. Phelan, Jr., A. J. Strauss, and R. H. Rediker, *Solid State Commun.* 2, 303 (1964).
3. J. F. Butler and A. R. Calawa, *J. Electrochem. Soc.* 112, 1056 (1965).
4. J. F. Butler, A. R. Calawa, and T. C. Harman, *Appl. Phys. Letters* 9, 427 (1966).
5. T. C. Harman, in "The Physics of Semimetals and Narrow-Gap Semiconductors", edited by D. L. Carter and R. T. Bate (Pergamon, Oxford, England, 1971), p. 363.
6. R. W. Ralston, I. Melngailis, A. R. Calawa, and W. T. Lindley, *IEEE J. Quantum Electron.* QE-9, 350 (1973).
7. P. Zoutendyk, Ph.D. Thesis, Calif. Inst. of Tech., 1968, unpublished.
8. H. Holloway, J. Nonmetals (to be published), other references to the materials growth can be found in this paper.
9. E. M. Logothetis, H. Holloway, A. J. Varga, and E. Wilkes, *Appl. Phys. Letters* 19, 318 (1971).
10. H. Holloway, W. H. Weber, E. M. Logothetis, A. J. Varga, and K. F. Yeung, *Appl. Phys. Letters* 21, 5 (1972).
11. P. K. Tien, *Appl. Opt.* 10, 2395 (1971).
12. D. H. Hensler, J. D. Cuthbert, R. J. Martin, and P. K. Tien, *Appl. Opt.* 10, 1937 (1971).
13. F. K. Reinhart, I. Hayashi, and M. B. Panish, *J. Appl. Phys.* 42, 4466 (1971).
14. D. F. Nelson and J. McKenna, *J. Appl. Phys.* 38, 4057 (1967).
15. M. Born and E. Wolf, "Principles of Optics" (Pergamon, New York, 1964), 2nd ed. pp. 61-70.
16. P. Beckmann and A. Spizzichino, "The Scattering of Electromagnetic Waves from Rough Surfaces", (Pergamon, Oxford, England, 1963).

REFERENCES (Cont'd.)

17. K. O. Hill, A. Watanabe, and J. G. Chambers, *Appl. Opt.* 11, 1952 (1972).
18. K. W. Nill, A. R. Calawa, T. C. Harman, J. N. Walpole, *Appl. Phys. Letters* 16, 375 (1970).
19. K. W. Nill, J. N. Walpole, A. R. Calawa, and T. C. Harman, in "The Physics of Semimetals and Narrow-Gap Semiconductors", edited by D. L. Carter and R. T. Bate (Pergamon, Oxford, England, 1971), p. 383.
20. E. R. Washwell and K. F. Cuff, "Radiative Recombination Symposium, Paris" (Academic, New York, 1964), p. 11.
21. G. Lasher and F. Stern, *Phys. Rev.* 133, A553 (1964).
22. J. M. Besson, W. Paul, and A. R. Calawa, *Phys. Rev.* 173, 699 (1968).
23. M. J. Adams and P. T. Landsberg, in "Gallium Arsenide Lasers", edited by C. H. Gooch (Wiley, New York, 1969), Chap. 2.
24. For a summary of the Pb-salt band parameters see R. Dalven, *Infrared Physics* 9, 141 (1969).
25. J. N. Zemel, J. D. Jensen, and R. B. Scholar, *Phys. Rev.* 140, A530 (1965).
26. I. G. Ferreira, *Phys. Rev.* 137, A1601 (1965).
27. P. G. McMullin, Ph.D. Thesis, Mass. Inst. of Tech., 1971, unpublished.
28. D. K. Hohnke, unpublished.
29. T. S. Moss, "Optical Properties of Semiconductors" (Butterworths, London, 1959), p. 30.
30. H. A. Lyden, *Phys. Rev.* 135, A514 (1964).

TABLE 1

THRESHOLD CHARACTERISTICS FOR THIN-FILM PbTe DIODE LASERS

Sample	Film Thickness μm	Cavity Length μm	Threshold Current Amp	$\alpha(E_m)$ cm^{-1}	α_{fc} cm^{-1}	$L^{-1}\lambda nR^{-1}$ cm^{-1}	α_s cm^{-1}	σ μm
242-3b	4.5	400	0.17	59	6.2	12	41	0.052
272-1a	3.2	400	0.41	200	1.2	10	189	0.059
299-3d	2.8	400	0.18	100	1	9.6	90	0.052
307-3a	2.4	180	0.13	188	1.3	20	167	0.053

-30.

FIGURE CAPTIONS

- Fig. 1 Geometry for PbTe waveguide on BaF_2 substrate.
- Fig. 2 Film thickness vs θ_c/ω for the low order modes. The dashed curves are solutions corresponding to no penetration of the fields into the surrounding media.
- Fig. 3 Power reflectivity vs film thickness for the first two TM and TE modes, calculated from the square of Eq. (9).
- Fig. 4 Power reflectivity for zero order modes vs the guide angle defined in the figure.
- Fig. 5 Surface scattering loss coefficient defined in Eq. (12) vs the film thickness for the first two TE and TM modes.
- Fig. 6 Gain enhancement factor defined in Eq. (17) vs the film thickness for the first two TE and TM modes.
- Fig. 7 Schematic drawing showing a completed sample. Since each Pb strip can be biased with either Pt contact, lasing can be obtained in this structure from four different optical cavities.
- Fig. 8 Scanning electron microscope photograph of two laser end reflectors. The samples have been potted in epoxy and lapped edgewise. In (a) the edge is defined by the photoresist technique. The light streak at the left is the Pb film. In (b) the edge is defined by a close-spaced evaporation mask.

FIGURE CAPTIONS (Cont'd.)

- Fig. 9 Spontaneous emission spectrum at 77°K. The dashed line is calculated from Eq. (21) with the peak rounded to indicate some residual attenuation. Device parameters: $p = 1.5 \times 10^{17} \text{ cm}^{-3}$, $d = 4.6 \mu\text{m}$, $L = 400 \mu\text{m}$.
- Fig. 10 Semilog plot of the spontaneous emission spectrum on the high energy side of the peak. The solid line is the slope predicted by Eq. (21). Device parameters: $p = 4.8 \times 10^{17}$, $d = 4.8 \mu\text{m}$, $L = 400 \mu\text{m}$.
- Fig. 11 Laser emission at 10°K for an annealed sample. The upper trace is near the laser threshold. The linewidths in each case are spectrometer resolution limited. The lower trace has twice the resolution, and the signal level is 40x larger than in the upper trace. Each set of 4 arrows is drawn with an 80 Å spacing. The peak in the upper trace coincides with the second arrow from the left. Device parameters: $p \approx 10^{18} \text{ cm}^{-3}$, $d = 2.4 \mu\text{m}$, $L = 400 \mu\text{m}$.
- Fig. 12 Pulsed laser emission at 9.5°K in an unannealed sample. The large splitting is roughly 1.4 meV. Device parameters: $p = 1.6 \times 10^{17} \text{ cm}^{-3}$, $d = 2.4 \mu\text{m}$, $L = 400 \mu\text{m}$.

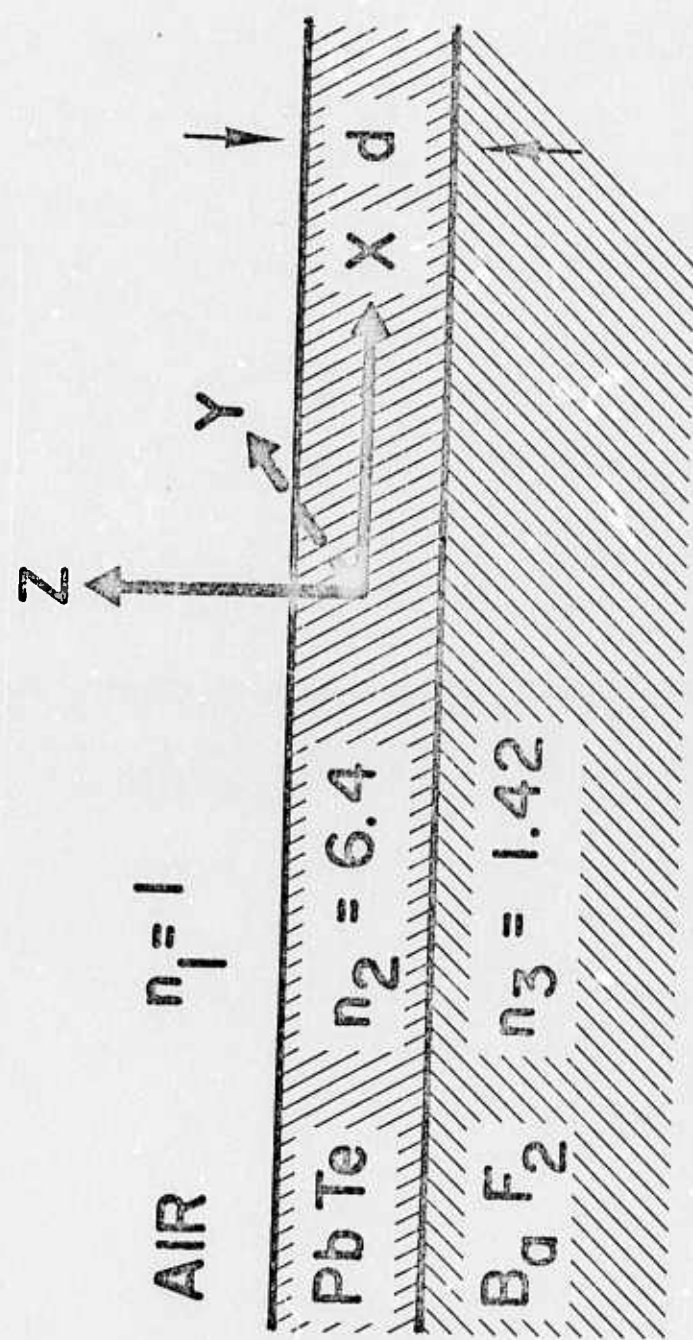


Fig. I

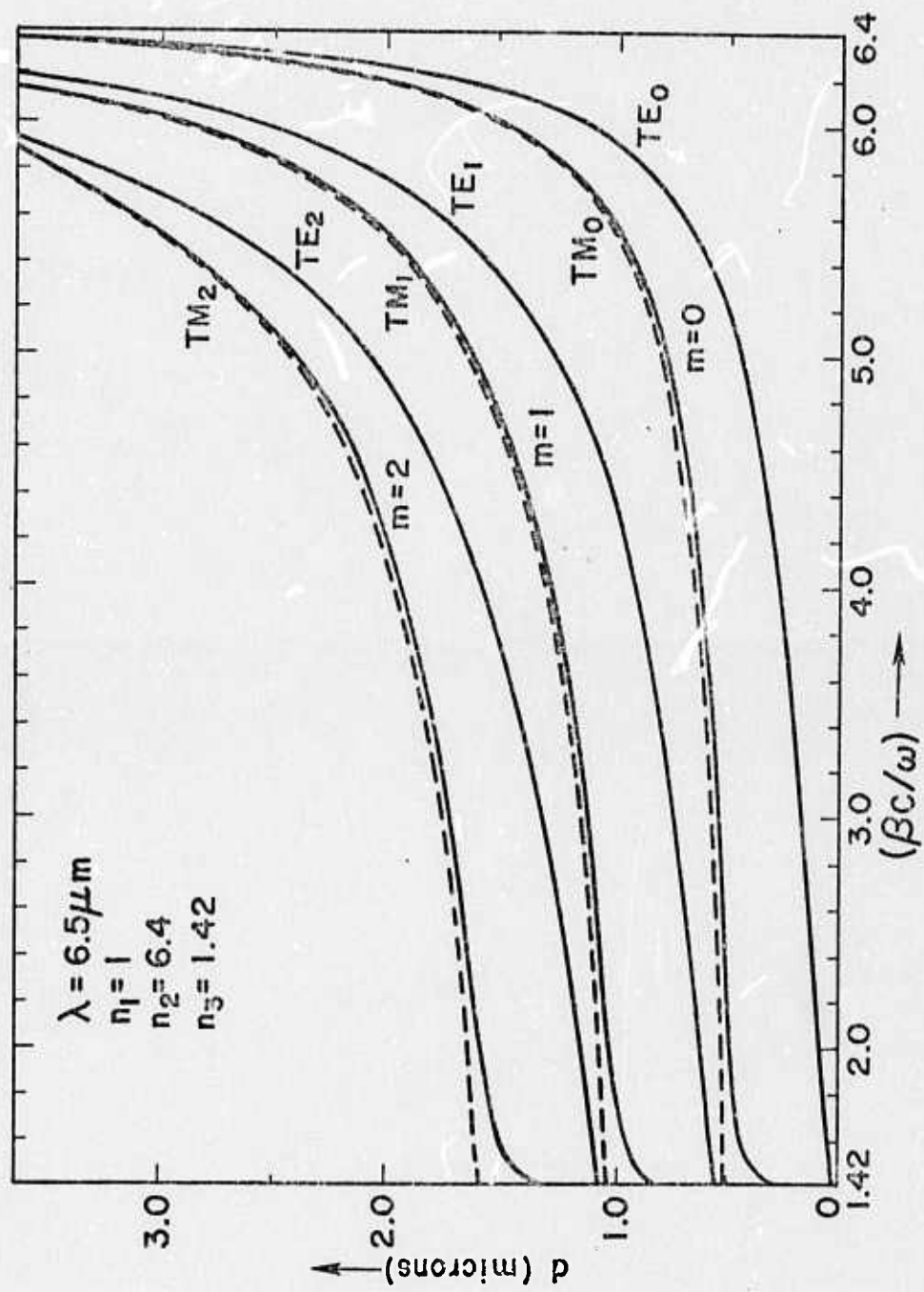


Fig.2

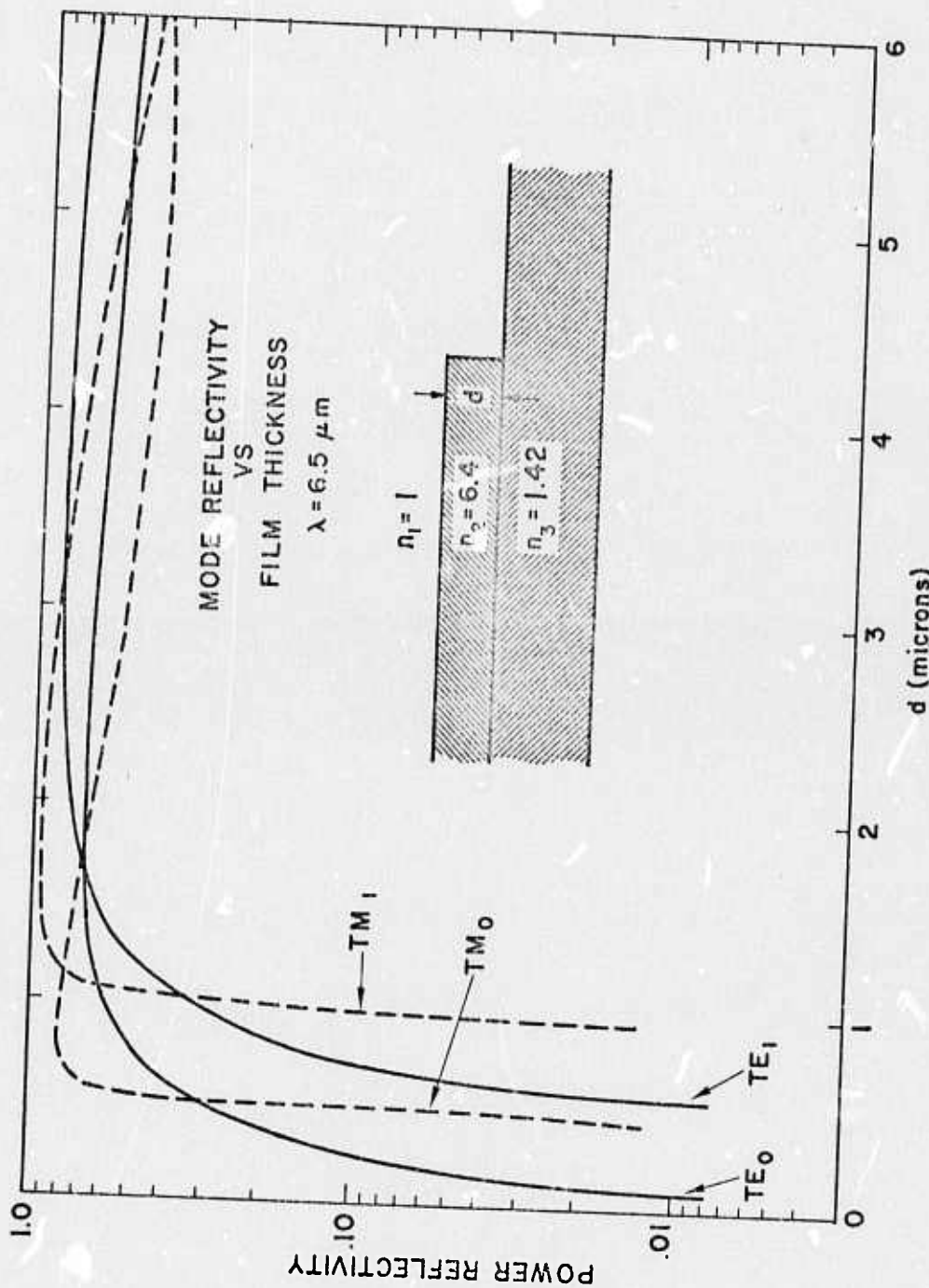


FIG. 3

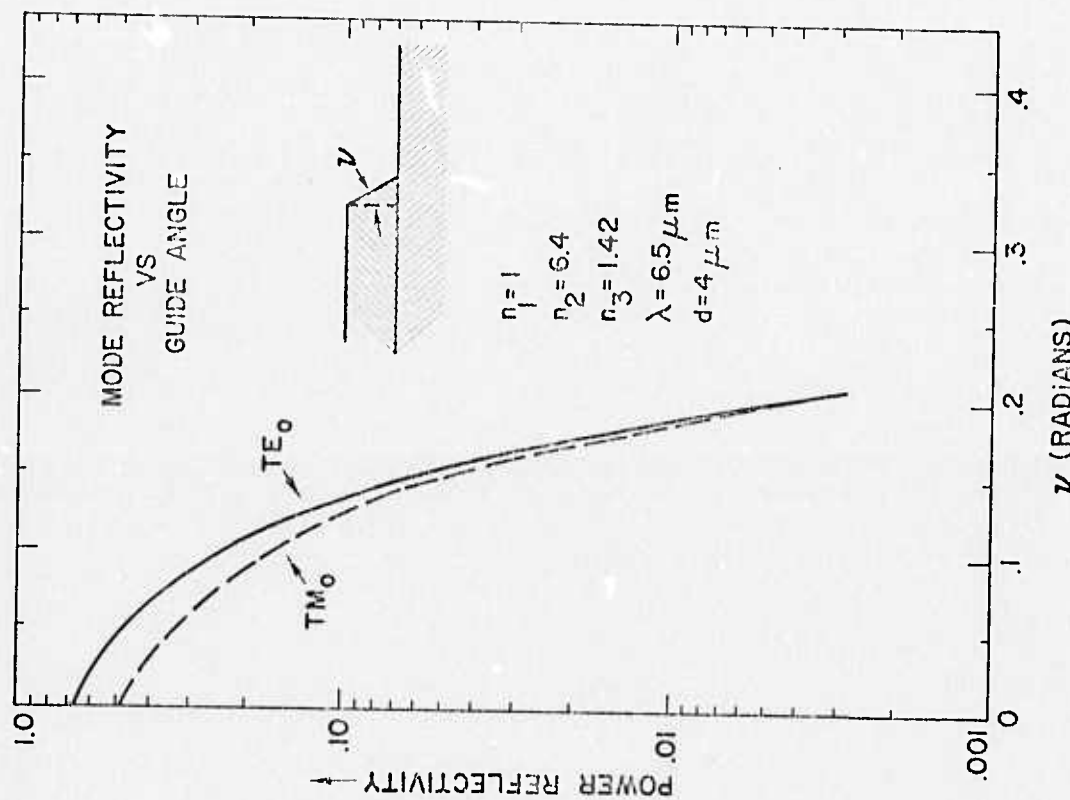


FIG. 4

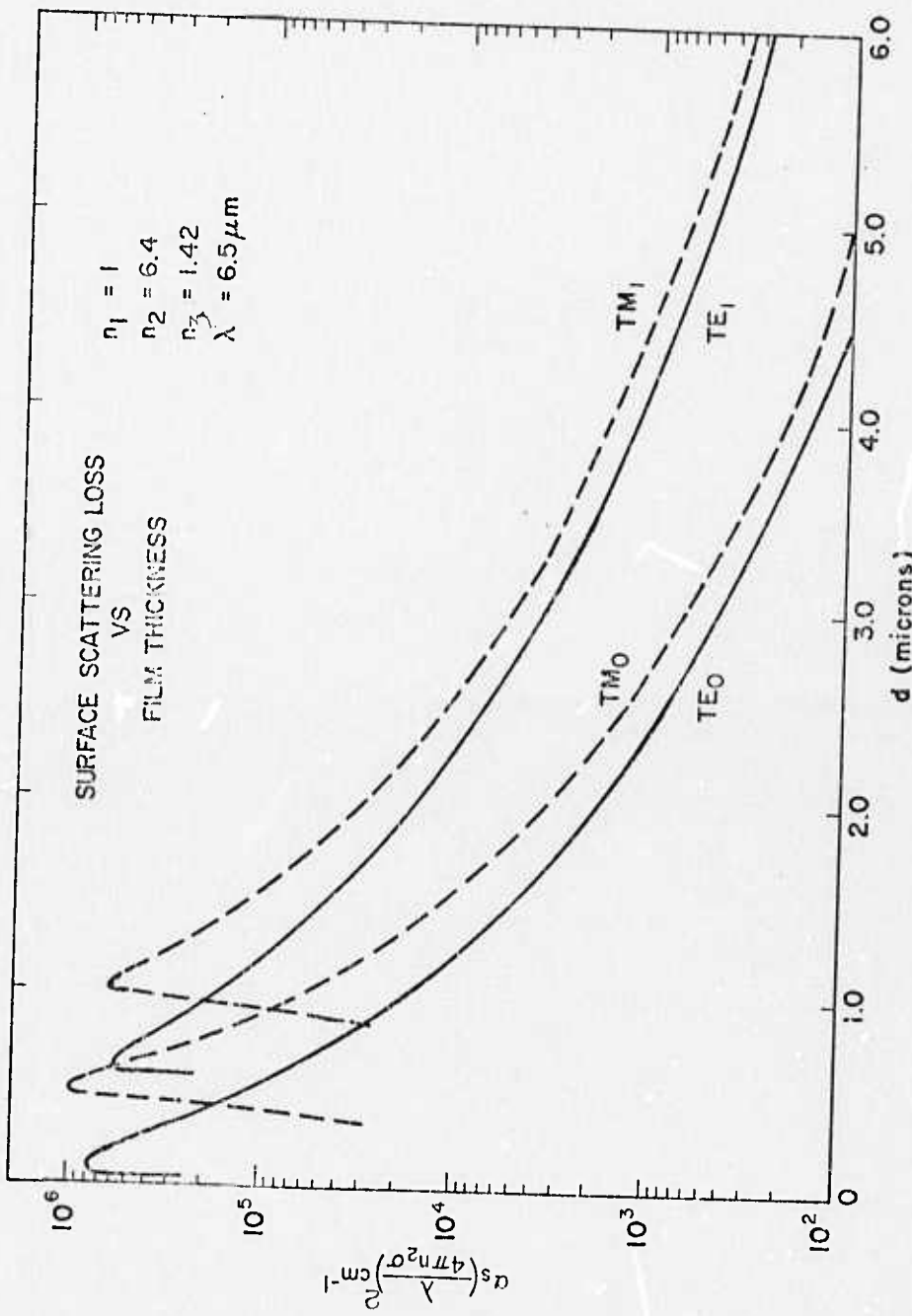


Fig. 5

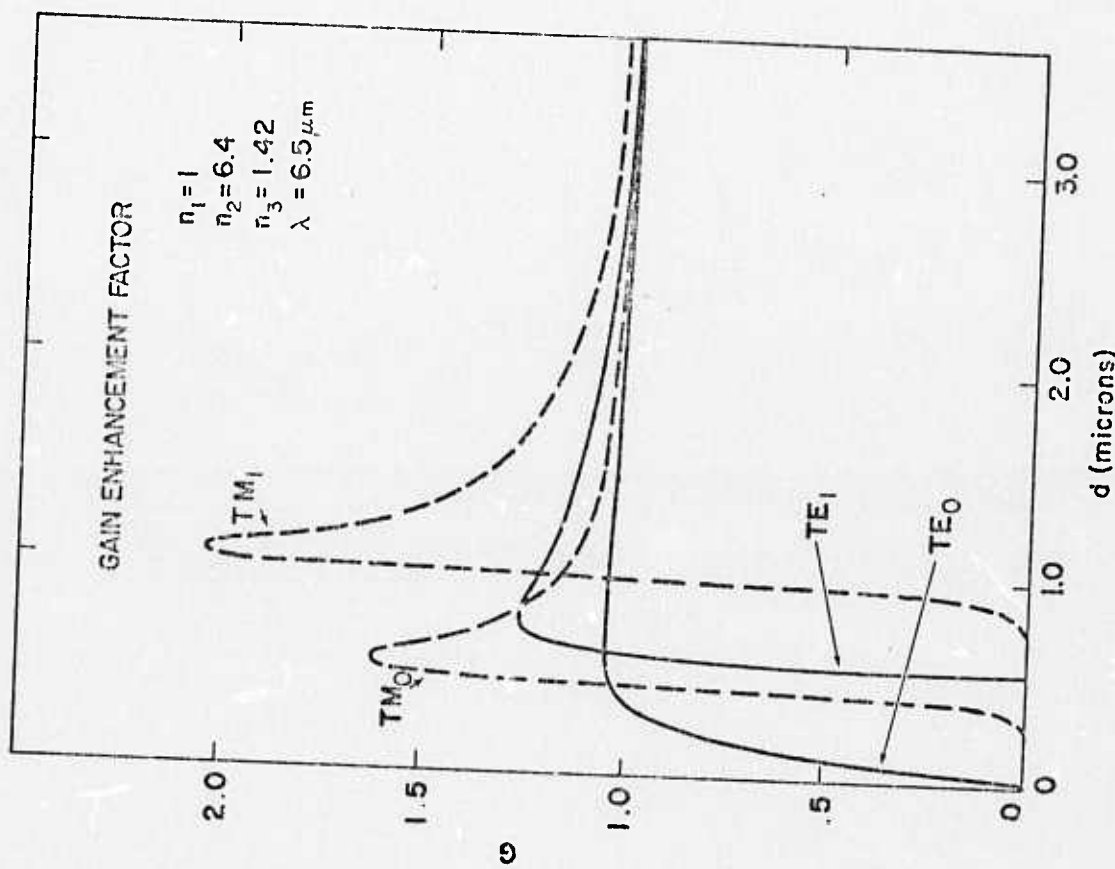


Fig. 6

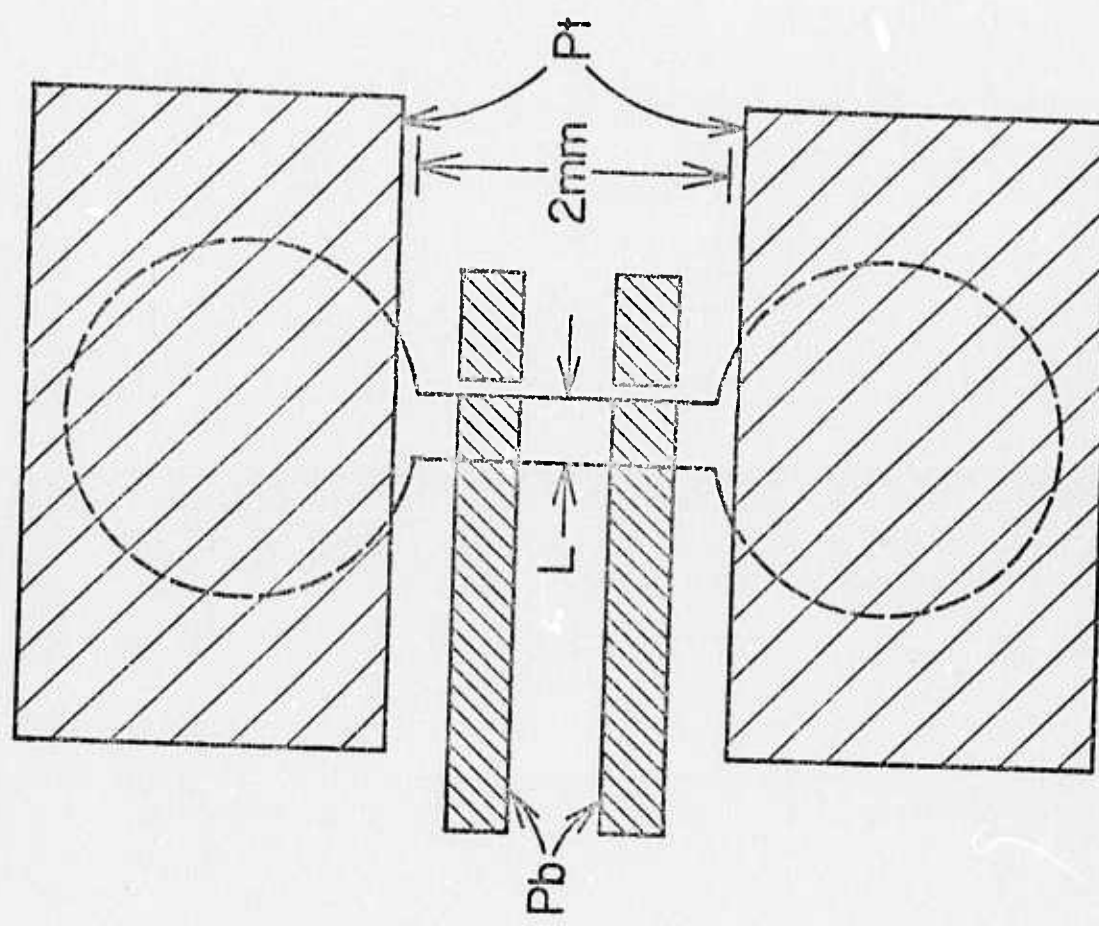


Fig. 7



(a)



(b)



Fig. 8

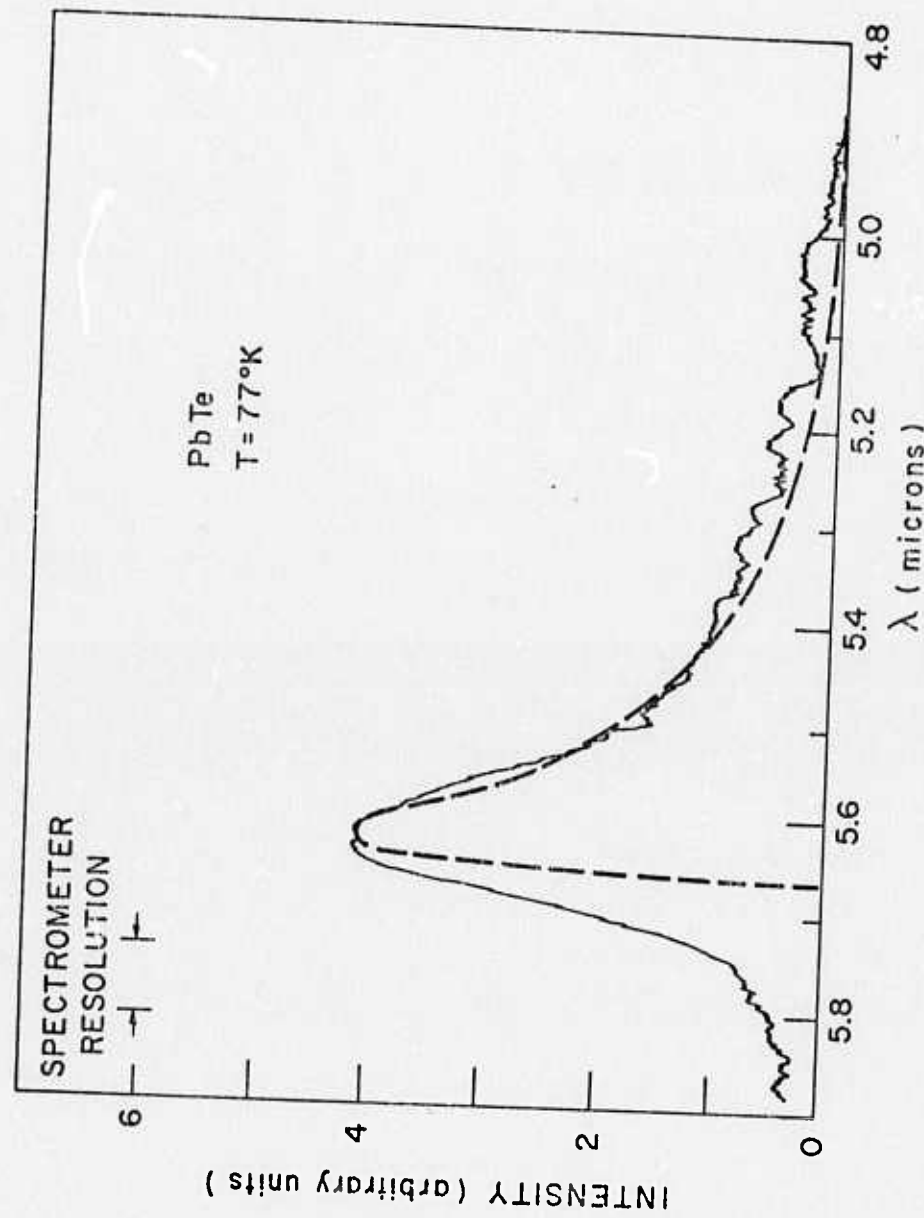


Fig. 9

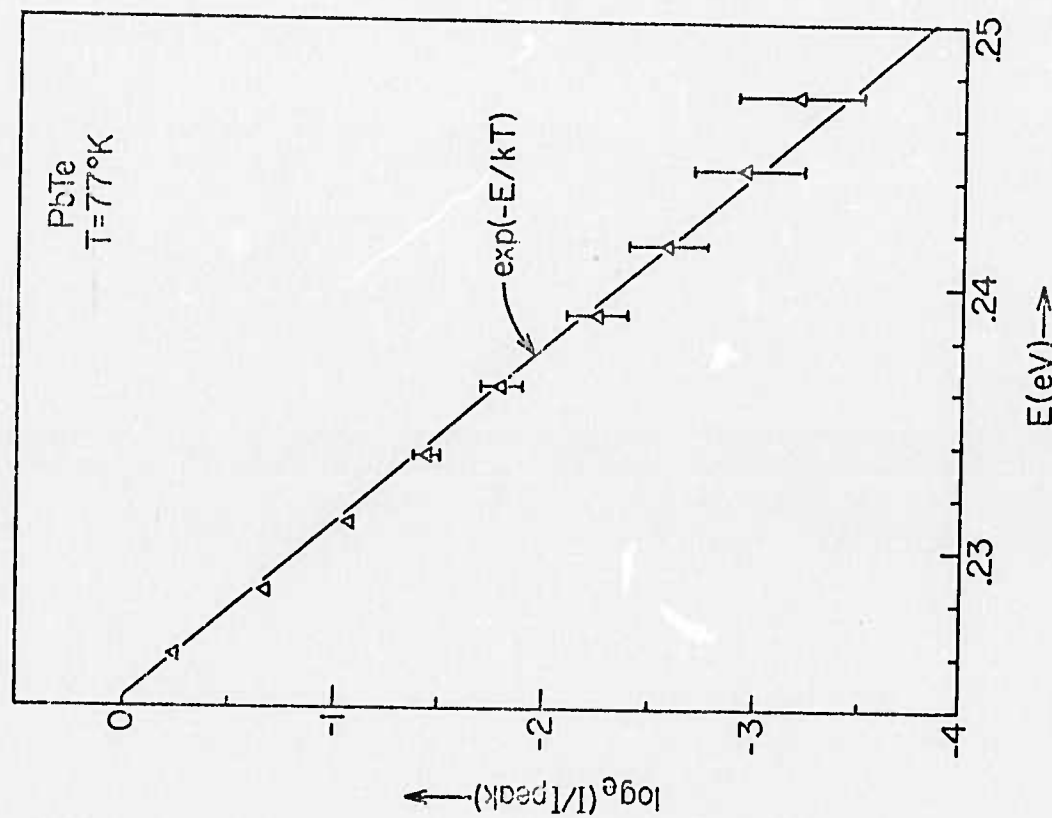


Fig. 10

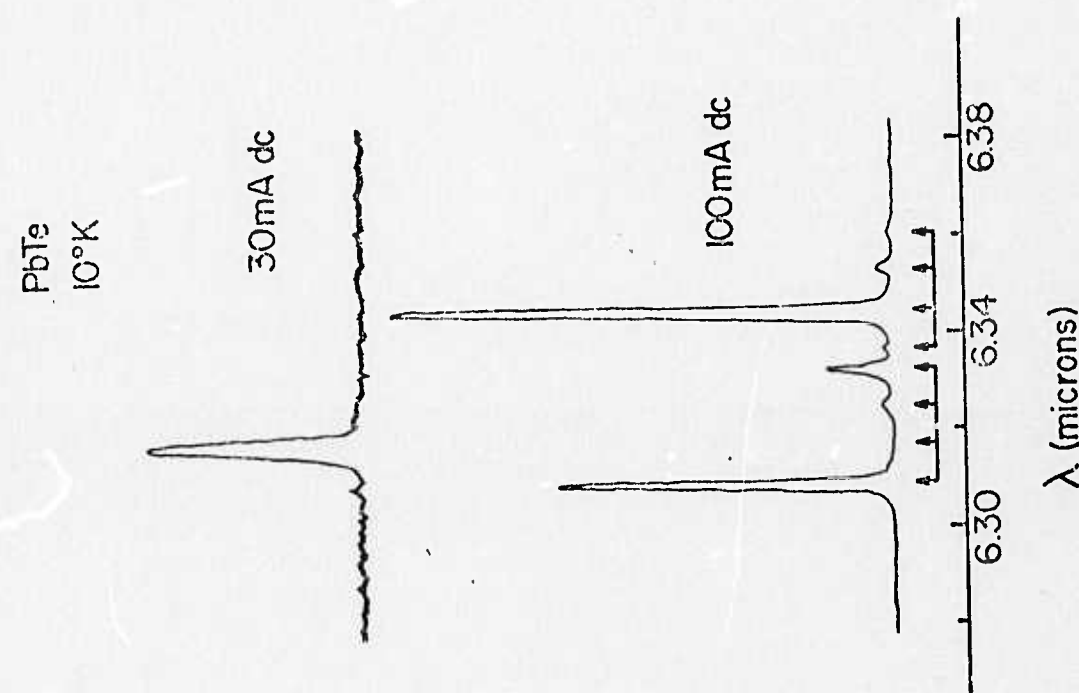


Fig. 11

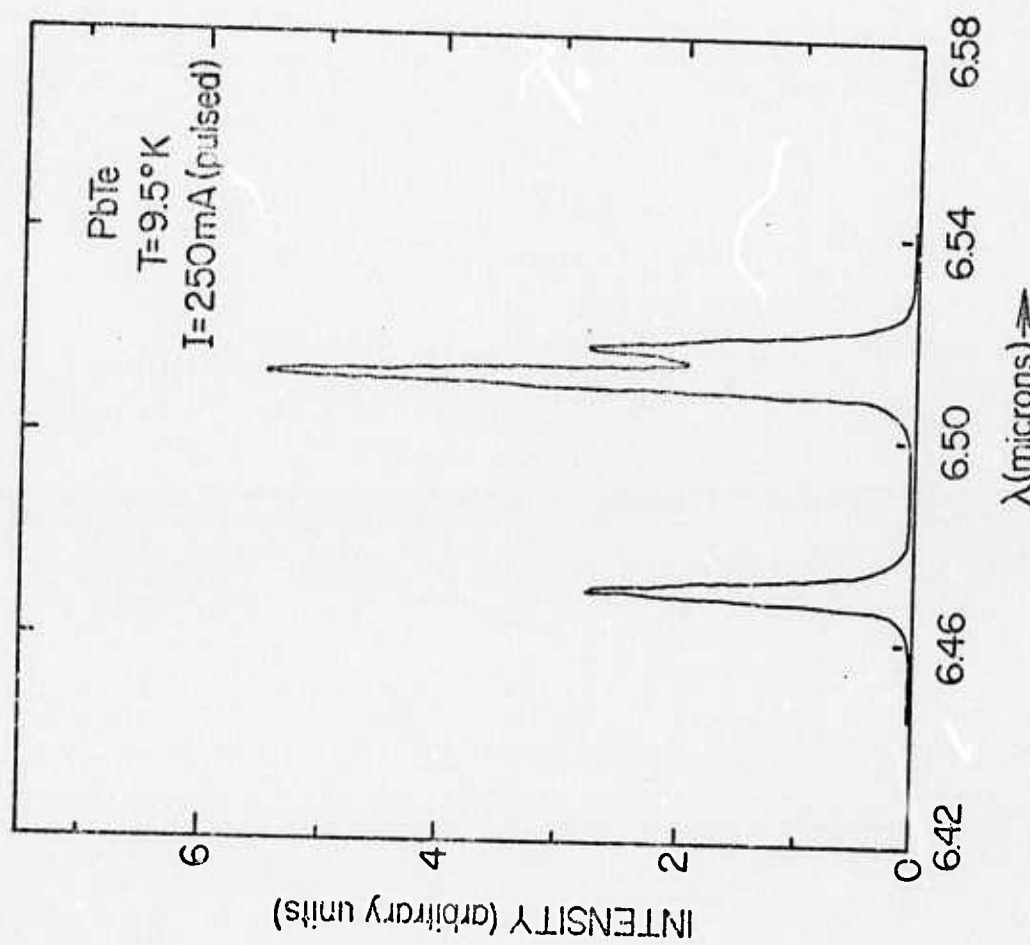


Fig. 12